RSC Advances

ROYAL SOCIETY OF CHEMISTRY

www.rsc.org/advances

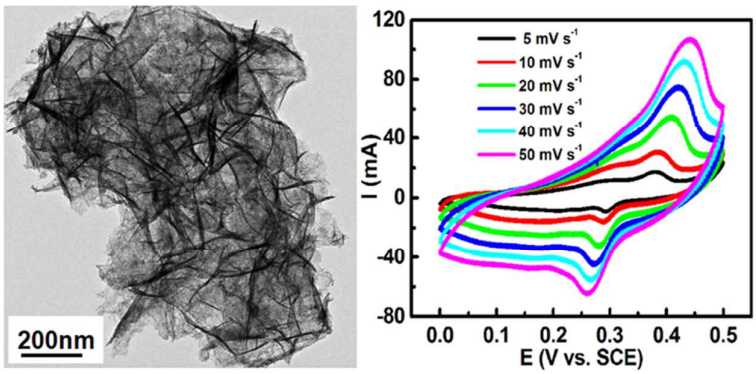

One-step alkaline hydrothermal strategy was developed to fabricate the strongly coupled Co_3O_4 NSs-rGO hybrid with large specific capacitance and high electrochemical utilization at high rates towards advanced supercapacitors.

One-step hydrothermal fabrication of strongly coupled Co_3O_4 nanosheets-reduced graphene oxide towards electrochemical capacitors

Changzhou Yuan,[a, b] Longhai Zhang,[a] Linrui Hou,[a] Gang Pang,[a] and Won-Chun Oh*[c]*

[a] School of Materials Science & Engineering, Anhui University of Technology, Ma□anshan, 243002, P.R. China

[b] Key Laboratory of Colloid and Interface Chemistry (Shandong University), Ministry of Education, Ji□nan, 250100, P.R. China

[c] Department of Advanced Materials Science & Engineering, Hanseo University, Seosan-si, Chungnam-do, 356-706, Korea

Email: ayuancz@163.com (C. Yuan); wc_oh@hanseo.ac.kr (W. Oh)

Abstract

In the work, we developed one-step synthetic strategy to prepare the strongly coupled Co_3O_4 nanosheets-reduced graphene oxide (Co_3O_4 NSs-rGO) hybrid, and further utilized it as a promising electroactive material for electrochemical capacitors (ECs). During the hydrothermal procedure, the GO was reduced and Co_3O_4 NSs were *in situ* grown onto the rGO sheets simultaneously due to the electrostatic interaction between the Co^{2+} and GO sheets. Electrochemical characteristics indicated that the Co_3O_4 NSs-rGO hybrid with ~7.2 wt.% Co_3O_4 loading delivered a specific capacitance (SC) of 187 F g^{-1} at 1.2 A g^{-1}. Furthermore, the SC degradations of the

hybrid were ~6 and 9% at constant current densities of 1.2 and 5 A g^{-1} after 1000 continuously charge-discharge cycles, demonstrating its desirable electrochemical stability. The synergetic effect of nanoscale size and good redox activity of the Co_3O_4 NSs combined with high electronic conductivity of the rGO resulted in the enhanced electrochemical utilization at high rates. In addition, an activated carbon/Co_3O_4 NSs-rGO asymmetric EC was further fabricated, and exhibited a specific energy density of ~13.4 Wh kg^{-1}, specific power density of ~2166 W kg^{-1} and striking electrochemical stability with ~11% SC degradation after 1000 cycles.

Key words: Co_3O_4 nanosheets; Reduced graphene oxide; Hydrothermal synthesis; Electrochemical capacitors

1. Introduction

Most recently, electrochemical capacitors (ECs), as a promising intermediate system between dielectric capacitors and conventional batteries, have drawn wide attention, due to their outstanding characteristics of fast energy delivery, short charging time, high power capability, long cycling life, and environment-friendly features.[1-3] It is such promising properties that make them intriguing energy-storage devices in a wide range of applications, including electric vehicles (EVs), HEVs, mobile electronic devices, memory backup systems, and so on. In general, ECs can be categorized into electrical double-layer capacitors (EDLCs) and pseudo-capacitors, depending upon the different charge storage mechanisms as well as the electroactive

materials used.[1] As both of the two have pluses and minuses, accordingly, enormous efforts were greatly stimulated to couple pseudo-capacitive materials with double-layer capacitive materials together for maximizing electrochemical performance in targeting high power and energy delivery capabilities meanwhile as a result of the synergetic mechanism both of EDLC and pseudo-capacitors.[4-6]

Of particular note, cobalt oxide (Co_3O_4) has been investigated well as a typical electroactive material among these Faradaic pseudo-capacitive transition metal oxides (TMOs), considering its low cost, natural abundance, environmental safety, *et al.*[7-10] Unfortunately, relatively poor electronic conductivity of the Co_3O_4 itself commonly results in modest specific capacitance (SC) and ineffective electrochemical utilization for ECs application. Various carbonaceous electrode materials, such as, carbon fibers,[11, 12] carbon nanotubes,[13] and otherwise, are thereby anticipated to enhance the electrochemical performance of the electroactive Co_3O_4 phase, thanks to their highly accessible surface area, good electronic conductivity, and superior chemical stability. On the other hand, it is worthy of noting that the reduced graphene oxide (rGO) is extensively considered as a fascinating "wonder land" perfect for integrating functional pseudocapacitve Co_3O_4 with special microstructure and morphologies.[7, 14-21] Nevertheless, a troublesome two-step method, particularly annealing at high temperature, is commonly necessary to grow nanosized and well-dispersed Co_3O_4 upon the rGO surface.[9, 15, 16, 22] Therefore, it is still challenging and imperative to explore more efficient yet even simpler ways to synthesize nanoscale Co_3O_4-rGO hybrid with improved electrochemical capacitance for advanced ECs.

Herein, we develop a facile but efficient strategy to fabricate strongly coupled Co_3O_4 nanosheets-rGO (donated as Co_3O_4 NSs-rGO hereafter) for ECs application *via* a simple one-step hydrothermal route. In essence, the method proposed here utilizes a facile one-pot hydrothermal route, yet it distinguishes itself from other conventional routes where the two-step process, even including high-temperature calcination, was generally applied. Afterwards, electrochemical performance of the hybrid Co_3O_4 NSs-rGO electrode is evaluated for high-performance ECs in a three-electrode system at room temperature (RT). And the as-prepared Co_3O_4 NSs-rGO hybrid exhibits striking SCs and good cycling stability at high rates in a 2 M KOH aqueous electrolyte. Furthermore, an asymmetric EC was fabricated, where activated carbon (AC) and Co_3O_4 NSs-rGO were used as the negative and positive electrodes, respectively, and delivered an excellent specific power density, attractive energy density and electrochemical stability.

2. Experimental

2.1. Synthesis of the hybrid Co_3O_4 NSs-rGO

All the chemicals were of analytical grade and directly used without further purification. Graphene oxide (GO) was prepared from natural graphite by a modified Hummers method as described elsewhere.[7, 23, 24] The as-synthesized GO was suspended in water to give a brown dispersion, which was then subjected to dialysis to completely remove residual salts and acids. In a typical synthesis of the hybrid Co_3O_4 NSs-rGO, firstly, 27 mg of GO and 7.5 mg of $Co(NO_3)_2{\cdot}6H_2O$ were dispersed into 32 mL de-ionized (DI) water by ultrasonication for 2 h to form uniform GO

solution. Secondly, 18 mL of $NH_3 \cdot H_2O$ was added into the mixed solution under stirring for 10 min. The reaction mixture was then transferred to a Teflon-lined autoclave and hydrothermally treated at 100 °C for 15 h. After cooled to RT, the solid product was obtained by filtering and washing with DI water and absolute ethanol for several times. For comparison, 5, 12.5 and 15 mg of $Co(NO_3)_2 \cdot 6H_2O$ was added during synthetic process to prepare another Co_3O_4-rGO hybrids, which were denoted as Co_3O_4-rGO-1, Co_3O_4-rGO-2 and Co_3O_4-rGO-3, respectively. Furthermore, without the addition of the Co species in the synthetic procedure, the rGO was also fabricated accordingly.

2.2. Materials characterization

The samples were examined by powder X-ray diffraction (XRD) (Max 18 XCE, Japan) using a Cu Ka source (λ = 0.154056 nm) at a scanning speed of 3° min^{-1} over a 2θ range of 10 – 80°. The morphologies and structures were observed with field-emission scanning electron microscopy (FESEM, JEOL-6300F, 15 kV) and transmission electron microscope (TEM) and high-resolution TEM (HRTEM) (JEOL JEM 2100 system operating at 200 kV).

2.3. Electrochemical tests

The working electrode was prepared by mixing 85 wt.% of the hybrid Co_3O_4 NSs-rGO, 5 wt.% of acetylene black (AB) and 10 wt.% of poly(tetrafluoroethylene) (PTFE), and then pressing the mixture onto a nickel grid (1 cm^2). The electrolyte used here was 2 M KOH aqueous solution. Electrochemical performance of the samples was evaluated at RT by cyclic voltammetry (CV) and chronopotentiometry (CP) tests

with an IVIUM electrochemical workstation (the Netherlands). The typical loading of the electroactive Co_3O_4 NSs-rGO hybrid is 5 mg cm^{-2}. The activated carbon (AC, Chenming Co., China) electrode was prepared by the same method as that of hybrid Co_3O_4 NSs-rGO electrode. All experiments were carried out in a three-electrode system with a working electrode, a platinum plate counter electrode (1 cm^2) and a saturated calomel electrode (SCE) reference electrode. And the cycling performance was carried out with a CT2001D tester (Wuhan, China). The SC of the hybrid Co_3O_4 NSs-rGO, and AC electrodes was calculated from the CP curves based on the following equation:

$$C = \frac{It}{\Delta V} \quad (1)$$

where C, I, t and ΔV are the SC (F g^{-1}) of the electrodes, the discharging current density (A g^{-1}), the discharging time (s) and the discharging potential range (V), respectively.

An asymmetric quasi-capacitor was further fabricated by using 5 mg of AC as negative electrode and 7 mg of the Co_3O_4 NSs-rGO hybrid as positive electrode face to face in 2 M KOH aqueous solution. And the specific energy density (E) and power density (P) of the asymmetric EC can be calculated by using the equation:

$$E = Pt = \frac{1}{2}C(\Delta V)^2 \quad (2)$$

3. Results and discussion

3.1. Characteristics of the resulting Co_3O_4 NSs-rGO sample

Fig. 1a presents the typical XRD pattern of the as-obtained GO product. As

evident, an intense and sharp peak is observed at 2θ = 11.3°, corresponding to the characteristic (001) diffraction peak of the GO. The interlayer spacing of 0.78 nm is much larger than that of natural graphite (~0.34 nm), due to the introduction of the oxygen-containing function groups on the graphite sheets.[25, 26] And the wide-angle XRD pattern of the hybrid Co_3O_4 NSs-rGO product, in which ~7.2 wt.% Co_3O_4 loading is delivered on the condition that the Co species is wholly converted into the Co_3O_4 phase, is shown in Fig. 1b. Attractively, the sharp peak at 2θ = 11.3° disappears after alkaline hydrothermal treatment at 100 °C for 15 h, which confirms that the GO has been successfully reduced, and the rGO is formed accordingly. In addition, other nine peaks at 18.8 º, 31.2 º, 36.7 º, 44.7 º, 55.6 º, 59.3 º, 65.2 º, 74.8 º, 78.9 º fully correspond to the typical reflections from (111), (220), (311), (400), (422), (551), (440), (620) and (622) crystal planes of the well-crystallized Co_3O_4 with a face-centered cubic structure (JCPDS Card No. 43-1003), respectively. Moreover, the low and broad diffraction peaks indicated the small size of the as-synthesized Co_3O_4 phase. These XRD data obviously presents the unambiguous fact that the hybrid Co_3O_4-rGO can be fabricated *via* such one-step facile alkaline hydrothermal route. Evidently, the alkaline hydrothermal treatment applied here not only facilities the reduction of the GO [7, 27, 28] but also renders the formation of the Co_3O_4 phase.

Fig. 2a shows the representative low-magnification TEM image of the resulting Co_3O_4 NSs-rGO sample. The unique hybrid possesses a typical NS micro-structure with rippled silk morphology, owing to its ultrathin feature. In addition, as observed in the higher-magnification TEM image (Fig. 2b), some Co_3O_4 NSs with dark color, as

marked by the red circles, are dispersed well upon the light-colored RGO surface. It is due to the electrostatic interaction between the Co^{2+} and GO sheets[21, 29] that the strongly coupled Co_3O_4 NSs-rGO hybrid was obtained. The HRTEM image taken from the dark regions is demonstrated in Fig. 2c. As evident, crystal fringes are clearly displayed, and the *d*-spacing is derived to be ~0.21 nm, corresponding to the spacing between (220) planes of the nanoscale Co_3O_4. And when 5 mg of $Co(NO_3)_2{\cdot}6H_2O$ was applied for preparing the Co_3O_4-rGO-1 product (~4.8 wt.% Co_3O_4 loading), even less Co_3O_4 NSs are observed upon the rGO surface (Fig. 3a). More interestingly, when the amount of $Co(NO_3)_2{\cdot}6H_2O$ used in the synthetic process is up to 12.5 mg, another distinct morphology is thus presented for the Co_3O_4-rGO-2 sample (~11.5 wt.% Co_3O_4 loading), as shown in Fig. 3b. Clearly, some spherical Co_3O_4 nanoparticles (NPs) of ~200 – 300 nm and even some Co_3O_4 NPs aggregations with the size range of ~600 – 800 nm are obviously located upon the rGO surface. Thereby, it is easy to conclude that the concentration of the Co^{2+} applied here plays a significant role in the elegant formation of the strongly coupled Co_3O_4 NSs-rGO hybrid.

3.2 Electrochemical behavior of the hybrid Co_3O_4 NSs-rGO electrode

The as-synthesized Co_3O_4-rGO hybrids are further fabricated as ECs electrodes, and first characterized with the CV technique in a three-electrode system with a 2 M KOH aqueous electrolyte. Representative CV curves of the hybrid Co_3O_4 NSs-rGO at various scan rates ranged from 5 to 50 mV s^{-1} are demonstrated in Fig. 4a. Obviously, a pair of well-defined redox peaks within the electrochemical window of 0.0 – 0.5 V

(*vs*. SCE) is found over the entire range of scan rates as indicated, suggesting that the distinguished capacitive characteristics are mainly governed by Faradaic redox reactions taking place on and/or near the electroactive surface of the unique Co_3O_4 NSs-rGO hybrid electrode, which is greatly distinct from the common EDLC characterized by nearly rectangular CV shapes. Notably, the electrochemical current subsequently increases while the CV shape almost keeps the same with the increase of the scan rates, suggesting good electrochemical capacitance of the unique hybrid electrode. Impressively, the peak potential shifts only ~50 mV for a 10-time increase in the scan rate, revealing the low polarization of the coupled Co_3O_4 NSs-rGO electrode. Also, the typical redox peaks observed here should be attributed to the electrochemical inter-transition of multi-valence Co species, *i.e.*, two sequential redox reactions taking place according to the following two expressions (3 and 4).[7, 10, 11, 14, 30]

$$Co_3O_4 + OH^- + H_2O \leftrightarrow 3CoOOH + e^- \quad (3)$$

$$CoOOH + OH^- \leftrightarrow CoO_2 + H_2O + e^- \quad (4)$$

Of particular note, both the electrochemical cathodic and anodic peak currents vary linearly with the sweep rates, as seen from the Fig. 4b. This demonstrates that the unique Co_3O_4 NSs-rGO hybrid electrode owns excellent power property, and the typical capacitive behavior is not diffusion controlled. [31-34]

Fig. 5a shows galvanostatic charge-discharge curves of the hybrid Co_3O_4 NSs-rGO electrode in a three-electrode system. The nonlinear CP curves further verify the typical pseudo-capacitive feature of the hybrid electrode, which is in good

agreement with the CV analysis mentioned above. Based on the CP plots presented in Fig. 5a, the SCs are calculated, and then depicted in Fig. 5b. Evidently, the SCs of the hybrid electrode at 1.2, 1.5, 2, 3, 4 and 5 A g^{-1} are 187, 182, 177, 169, 162 and 152 F g^{-1}, respectively, much higher than that of 163.8 F g^{-1} (at 1 A g^{-1}) for the Co_3O_4-rGO scrolls in recent report.[35] And ~81% of the SC is also retained with the current density increases from 1.2 to 5 A g^{-1}, showing its appealing rate performance. In particular, as for other Co_3O_4-rGO hybrid electrodes with even more Co_3O_4 loadings, as seen in the inset in Fig. 5b, the Co_3O_4-rGO-2 and Co_3O_4-rGO-3 (~13.3 wt.% Co_3O_4 loading) samples just deliver a SC of 135 and 142 F g^{-1} at a current density of 1.2 A g^{-1}, and ~72% and 67% of SC retention are observed for the Co_3O_4-rGO-2 and Co_3O_4-rGO-3 products the when the current density increases up to 5 from 1.2 A g^{-1}, the reasons for which should be related to the larger size of the Co_3O_4 NPs and the second aggregation of Co_3O_4 NPs in these hybrids. And for the hybrid Co_3O_4-rGO-1, a SC of 156 F g^{-1} was obtained at a current density of 1.2 A g^{-1}, less than that of the strongly coupled Co_3O_4 NSs-rGO, due to the less loading of electroactive Co_3O_4. And the SC value is even higher than those of the Co_3O_4-rGO-2 and Co_3O_4-rGO-3 samples with much more Co_3O_4 loadings, for which the much larger naked electrochemical surface area of the Co_3O_4-rGO-1 should be responsible. More importantly, in such electrochemically working window, a modest SC of ~11 F g^{-1} is for the rGO at 2 A g^{-1} (Fig. S1, ESI†), similar to the reported before.[7, 20] As a consequence, the SCs calculated here for the Co_3O_4 NSs-rGO hybrid is mainly contributed by the pseudo-capacitive Co_3O_4 NSs, and the SCs of the Co_3O_4 NSs thus can be estimated as

~2300 F g^{-1} at a current density of 2 A g^{-1}, considering ~7.2 wt.% of the Co_3O_4 loading in the hybrid Co_3O_4 NSs-rGO. These data mentioned above strongly support the fact that the hybrid Co_3O_4 NSs-rGO is a promising electrode for ECs application due to its striking ability to deliver large SCs and high electrochemical utilization at high charge-discharge rate, which might be related to the striking structural features of the present hybrid electrode. Firstly, the rGO exiting in the unique hybrid enhances the electronic conductivity of the hybrid, prevents the agglomeration of the Co_3O_4 NSs, and increases the effective interfacial area between the Co_3O_4 NSs and the electrolyte during the electrochemical reaction. Secondly, the nanoscale size of the obtained Co_3O_4 NSs can reduce the diffusion length over which the OH^- must transfer during the charge-discharge process. It is the synergetic interaction between the rGO and Co_3O_4 NSs that renders its improved electrochemical capacitance even at large current densities.

The cycling stability of the strongly coupled Co_3O_4 NSs-rGO hybrid electrode is further evaluated by the repeated charging-discharging measurement at current densities of 1.2 and 5 A g^{-1} in a 2 M KOH aqueous solution, respectively, as shown in Fig. 6. Obviously, the SC is around 186 F g^{-1} in the first cycle and it gradually decreases to 175 F g^{-1} after cycling for 1000 times at a current density of 1.2 A g^{-1}, corresponding to a SC loss of only ~6%. And of particular note, the SC retention of 9% even can be achieved at a large current density of 5 A g^{-1}, which is good among TMOs-based nanostructure electrode materials.

3.3 Electrochemical performance of the AC/Co_3O_4 NSs-rGO asymmetric EC

To further highlight its application as a promising positive electrode for ECs, we fabricated an asymmetric EC by using AC with electrical double-layer capacitance as negative electrode (Fig. S2, ESI†) and the as-synthesized Co_3O_4 NSs-rGO as positive electrode, respectively. The typical I-E response of the asymmetric EC is presented in Fig. 7a, and shows well-defined mirror shape with the respect to the zero-current line and rapid current response on voltage reversal at each potential. Moreover, the upper voltage limit of the CV curves can be extended to 1.45 V, Which is of great significance to the enhancement of specific energy density and practical commercial interest. Fig. 7b demonstrates the galvanostatic CP plots of the AC/Co_3O_4 NSs-rGO asymmetric EC at a current density of 1 A g^{-1} in the potential range from 0 to 1.45 V. In addition, a nearly linear variation of the voltage is observed during the charge-discharge process, proving appealing capacitive behavior of the asymmetric EC. And a SC is calculated as ~42 F g^{-1} for such asymmetric EC according to the data shown in Fig. 7b. In addition, when the current density is up to 3 A g^{-1} (Fig. S3, ESI†), a SC of 33 F g^{-1} is still obtained, and a maximum SC of 46 F g^{-1} can be delivered at a current density of 0.25 A g^{-1}.

Furthermore, the Ragone plot of the AC/Co_3O_4 NSs-rGO asymmetric EC is shown in Fig. 8a, and illustrates the corresponding energy/power densities. The data of Fig. 8a clearly demonstrates that the asymmetric EC possesses good specific energy density and power density. Strikingly, the asymmetric EC is capable of delivering a high energy density of ~13.4 Wh kg^{-1} and an appealing power density of ~2166 W kg^{-1}, which is even comparable to other systems.[36-38] The long-term

cyclability is of great significance for EC application. Accordingly, the cycling behavior of the symmetric EC during charge-discharge process at 1 A g^{-1} for continuous 1000 cycles without relaxation is performed within the electrochemical window from 0.0 to 1.45 V. As shown in Fig. 8b, the SC of the symmetric EC decreases with the growth of the cycle number, and after continuous 1000 cycles, the capacitance value remains ~89% of that of the first cycle. The capacitance attenuation of ~11% suggests the good electrochemical stability of the symmetric EC.

4. Conclusions

In summary, an efficient one-pot hydrothermal strategy was proposed to fabricate the strongly coupled Co_3O_4 NSs-rGO hybrid. During the hydrothermal reaction, the GO was reduced, and the Co_3O_4 NSs were *in situ* grown onto the rGO NSs simultaneously due to the electrostatic interaction between the Co^{2+} and GO NSs. When further utilized as high-performance positive material for ECs, the hybrid Co_3O_4 NSs-rGO with ~7.2 wt.% of the Co_3O_4 NSs loading delivered a SC of 187 F g^{-1} at 1.2 A g^{-1}, and 151 F g^{-1} even at a large current density of 5 A g^{-1}. Appealing, the SC retention of the hybrid are ~94 and 91% after continuously cycling for 1000 times at 1.2 and 5 A g^{-1}, respectively, strongly revealing its striking electrochemical stability. The existence of rGO in the hybrid was anticipated to prevent the agglomeration of the Co_3O_4 NSs, enhance the electronic conductivity of the hybrid electrode, and increase the contact surface between the Co_3O_4 NSs and the electrolyte during the electrochemical reaction, which synergistically contributed to the enhanced electrochemical utilization of the unique Co_3O_4 NSs-rGO electrode even at high rates.

Furthermore, an AC/Co_3O_4 NSs-rGO asymmetric EC exhibited an attractive specific energy density, high power density and desirable cycling performance.

Acknowledgements The authors gratefully acknowledge the support by National Natural Science Foundation of China (no. 51202004), Natural Science Foundation of Anhui Province (no. 10040606Q07), and the Foundation of Key Laboratory of Colloid and Interface Chemistry (Shangdong University), Ministry of Education (no. 201201).

References:

[1] B. E. Conway, Electrochemical Supercapcitors: Scientific Fundamentals and Technological Applications, Plenum, New York 1999, Ch. 15.

[2] G. P. Wang, L. Zhang and J. J. Zhang, *Chem. Soc. Rev.*, 2012, **41**, 797.

[3] P. Simon and Y. Gogotsi, *Nat. Mater.*, 2008, **7**, 845.

[4] C. Z. Yuan, B. Gao, L. F. Shen, S. D. Yang, L. Hao, X. J. Lu, F. Zhang, L. J. Zhang and X. G. Zhang, *Nanoscale*, 2011, **3**, 529.

[5] M. J. Zhi, C. C. Xiang, J. T. Li, M. Li and N. Q. Wu, *Nanoscale*, 2013, **5**, 72.

[6] S. Bose, T. Kuila, A. K. Mishra, R. Rajasekar, N. H. Kim and J. H. Lee, *J. Mater. Chem.*, 2012, **22**, 767.

[7] C. Z. Yuan, L. Yang, L. R. Hou, J. Y. Li, Y. X. Sun, X. G. Zhang, L. F. Shen, X. J. Lu, S. L. Xiong and X. W. Lou, *Adv. Funct. Mater.*, 2012, **22**, 2560.

[8] S. Vijayakumar, A. K. Ponnalagi, S. Nagamuthu and G. Muralidharan, *Electrochim. Acta*, 2013, **106**, 500.

[9] S. Park and S. Kim, *Electrochim. Acta*, 2013, **89**, 516.

[10] C. Z. Yuan, L. Yang, L. R. Hou, L. F. Shen, F. Zhang, D. K. Li and X. G. Zhang, *J. Mater. Chem.*, 2011, **21**, 18183.

[11] F. Zhang, C. Z. Yuan, J. J. Zhu, J. Wang, X. G. Zhang and X. W. Lou, *Adv. Funct. Mater.*, 2013, **23**, 3909.

[12] L. Yang, S. Cheng, Y. Ding, X. B. Zhu, Z. L. Wang and M. L. Liu, *Nano Lett.*, 2012, **12**, 321.

[13] J. W. Lang, X. B. Yan and Q. J. Xue, *J. Power Sources*, 2011, **196**, 7841.

[14] C. C. Xiang, M. Li, M. J. Zhi, A. Manivannan and N. Q. Wu, *J. Power Sources*, 2013, **226**, 65.

[15] L. Wang, D. L. Wang, J. S. Zhu and X. S. Liang, *Ionics*, 2013, **19**, 215.

[16] J. Yan, T. Wei, W. M. Qiao, B. Shao, Q. K. Zhao, L. J. Zhang and Z. J. Fan, *Electrochim. Acta*, 2010, **55**, 6973.

[17] G. J. Liu, L. Q. Fan, F. D. Yu, J. H. Wu, L. Liu, Z. Y. Qiu and Q. Liu, *J. Mater. Sci.*, 2013, **48**, 8463.

[18] J. J. Yuan, J. W. Zhu, H. P. Bai, X. Q. Meng, S. M. Liang, L. L. Zhang and X. Wang, *Phys. Chem. Chem. Phys.*, 2013, **15**,12940.

[19] B. Wang, Y. Wang, J. Park, H. Ahn and G. Wang, *J. Alloys Compd.*, 2011, **509**,7778.

[20] D. H. Zhang and W. B. Zou, *Curr. Appl. Phys.*, 2013, **13**, 1796.

[21] G. Y. He, J. H. Li, H. Q. Chen, J. Shi, X. Q. Sun, S. Chen and X. Wang, *Mater. Lett.*, 2012, **82**, 61.

[22] S. Park, S. J. Park and S. Kim, *Bull. Korean Chem. Soc.*, 2012, **33**, 4274.

[23] J. Yan, T. Wei, W. M. Qiao, B. Shao, Q. K. Zhao, L. J. Zhang and Z. J. Fan, *Electrochim. Acta*, 2010, **55**, 6973.

[24] S. Stankovich, D. A. Dikin, R. D. Piner, K. A. Kohlhaas, A. Kleinhammes, Y. Y. Jia, Y. Wu, S. T. Nguyen and R. S. Ruoff, *Carbon*, 2007, **45**, 1558.

[25] C. Xu, X. Wu, J. Zhu and X. Wang, *Carbon*, 2007, **46**, 386.

[26] S. Chen, J. W. Zhu, X. D. Wu, Q. F. Han and X. Wang, *ACS Nano*, 2010, **4**, 2822.

[27] R. R. Wang, J. Sun, L. Gao, C. H. Xu, J. Zhang and Y. Q. Liu, *Nanoscale*, 2011,

3, 904.

[28] X. B. Fan, W. C. Peng, Y. Li, X. Y. Li, S. L. Wang, G. L. Zhang and F.B. Zhang, *Adv. Mater.*, 2008, **20**, 4490.

[29] S. M. Cui, S. Mao, G. H. Lu and J. H. Chen, *J. Phys. Chem. Lett.*, 2013, **4**, 2441.

[30] L. R. Hou, C. Z. Yuan, L. Yang, L. F. Shen, F. Zhang and X. G. Zhang, *RSC Adv.*, 2011, **1**, 1521.

[31] T. Brezesinski, J. Wang, S. H. Tolbert and B. Dunn, *Nat. Mater.*, 2010, **9**, 146

[32] C. Z. Yuan, J. Y. Li, L. R. Hou, J. D. Lin, X. G. Zhang and S. L. Xiong, *J. Mater. Chem. A*, 2013, **1**, 11145.

[33] A. J. Bard and L. R. Faulkner, Electrochemical Methods Fundamentals and Applications, 2nd ed., John Wiley, Inc, New York 2001, Ch. 6, P. 233, 235.

[34] Y. G. Wang, Z. S. Hong, M. D. Wei and Y.Y. Xia, *Adv. Funct. Mater.*, 2012, **22**, 5185.

[35] W. W. Zhou, J. P. Liu, T. Chen, K .S. Tan, X. T. Jia, Z. Q. Luo, C. X. Cong, H. P. Yang, C. M. Li and T. Yu, *Phys. Chem. Chem. Phys.*, 2011, **13**, 14462.

[36] C. Z. Yuan, B. Gao and X. G. Zhang, *J. Power Sources*, 2007, **173**, 606.

[37] Y. G. Wang and Y. Y. Xia, Electrochem. Commun., 2005, 7, 1138.

[38] Q. Wang, Z. H. Wen and J. H. Li, Adv. Funct. Mater., 2006, 16, 2141.

Captions and Figures

Fig. 1. Wide-angle XRD patterns of (a) the GO and (b) as-fabricated Co_3O_4 NSs-rGO product

Fig. 2. (a) TEM and (b) HRTEM images of the strongly coupled Co_3O_4 NSs-rGO sample

Fig. 3. (a) TEM image of the Co_3O_4-rGO-1 sample and (b) FESEM image of the Co_3O_4-rGO-2 sample

Fig. 4. (a) CV curves at various scan rates and (b) the relationship between peak current (i_p) and the sweep rate (v) of the resulting hybrid Co_3O_4 NSs-rGO

Fig. 5. (a) Charge-discharge curves (E *vs.* time) and (b) calculated SC as a function of current density for the Co_3O_4 NSs-rGO hybrid sample. The inset for the SC *via* current density for other Co_3O_4-rGO hybrids as indicated

Fig. 6. Cycling performance of the hybrid Co_3O_4 NSs-rGO sample at different current densities as indicated

Fig. 7. (a) CV curves (10 mV s^{-1}) and (b) charge-discharge plots (1 A g^{-1}) of the AC/Co_3O_4 NSs-rGO asymmetric EC

Fig. 8. (a) Ragone plot and (b) cycling behavior (1 A g^{-1}) of the AC/Co_3O_4 NSs-rGO asymmetric EC

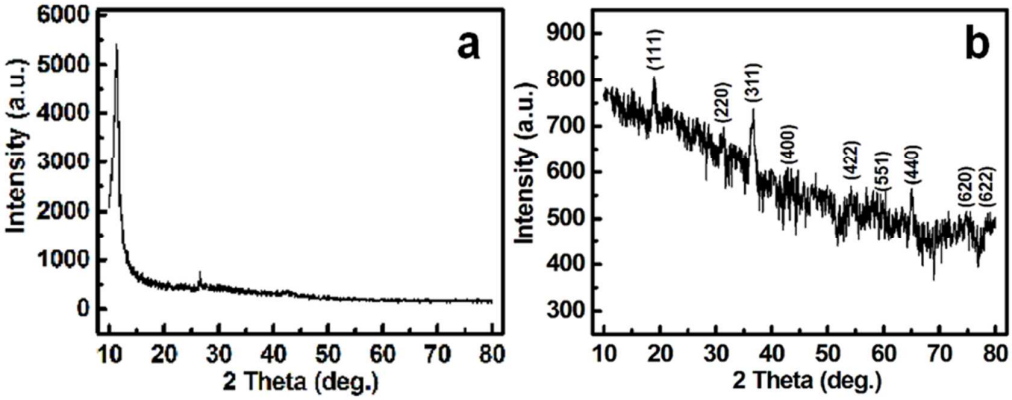

Figure 1 by Changzhou Yuan, *et al.*

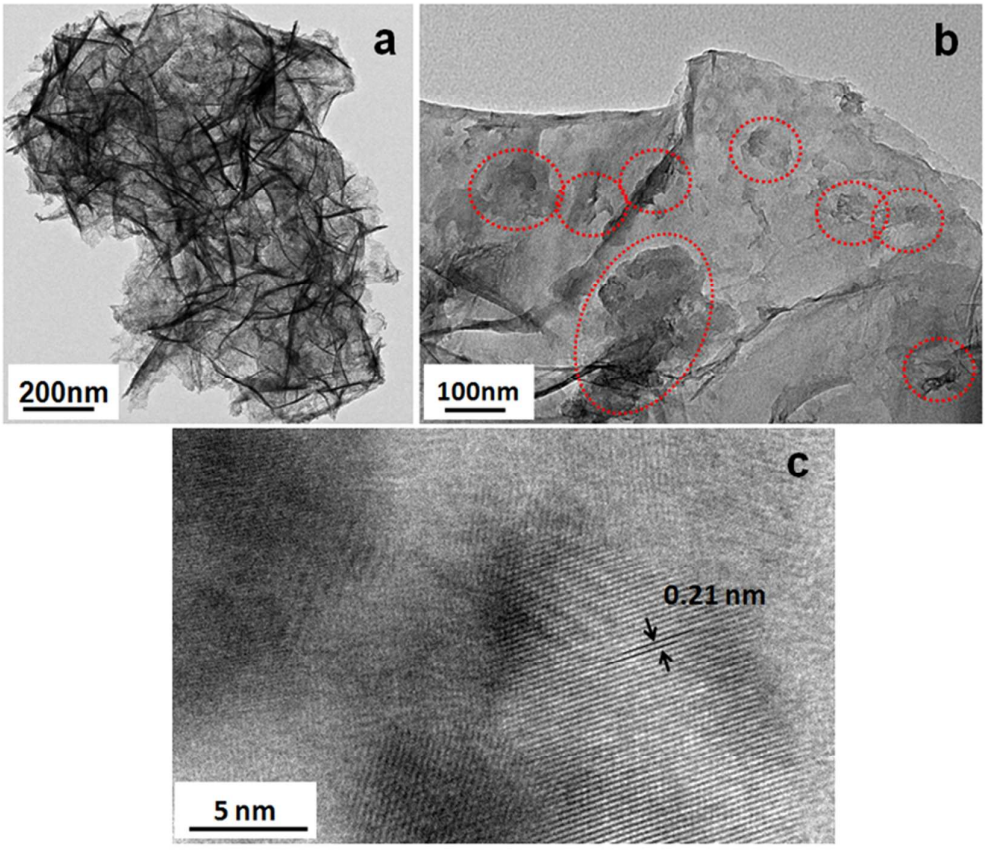

Figure 2 by Changzhou Yuan, *et al*.

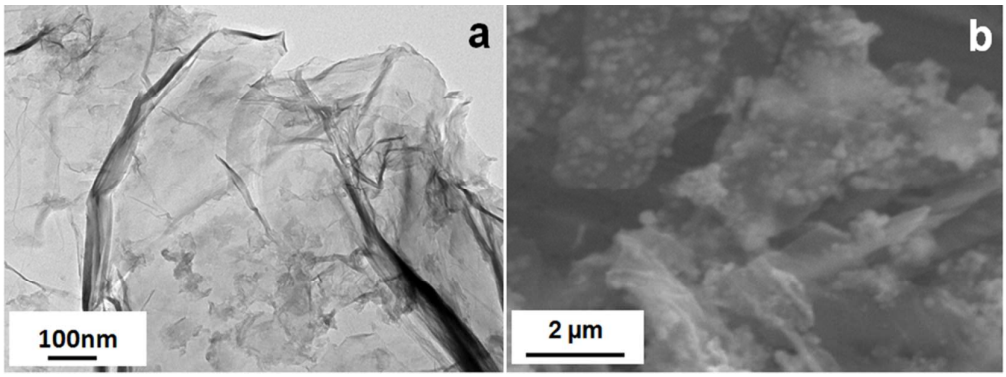

Figure 3 by Changzhou Yuan, *et al*.

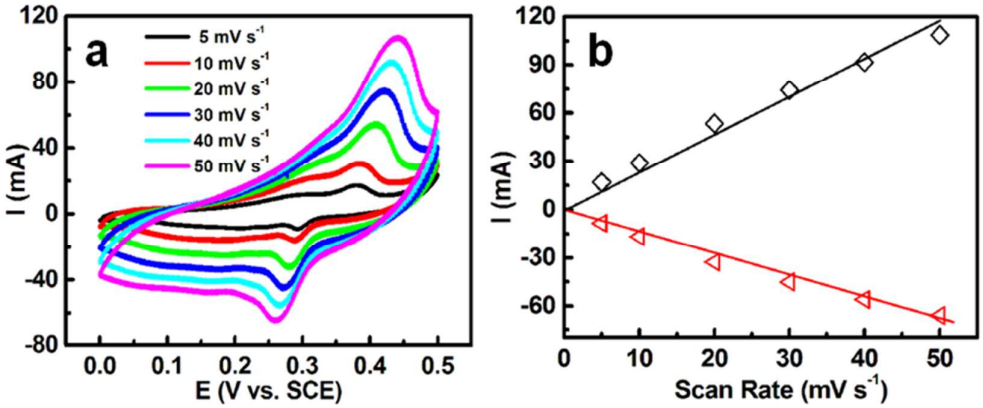

Figure 4 by Changzhou Yuan, *et al*.

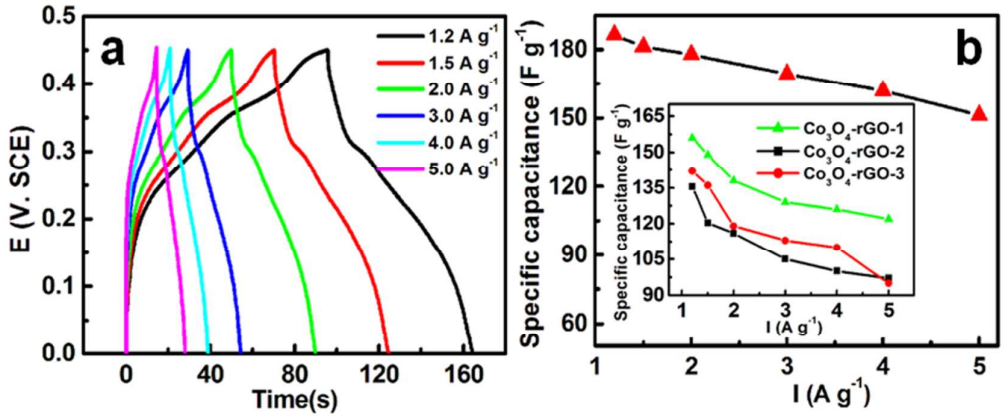

Figure 5 by Changzhou Yuan, *et al*.

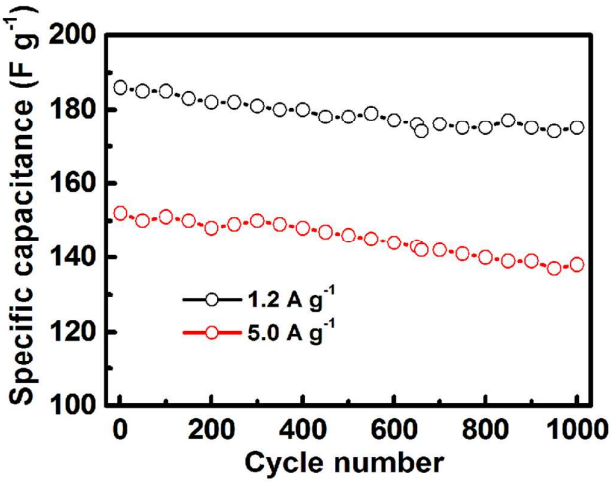

Figure 6 by Changzhou Yuan, *et al*.

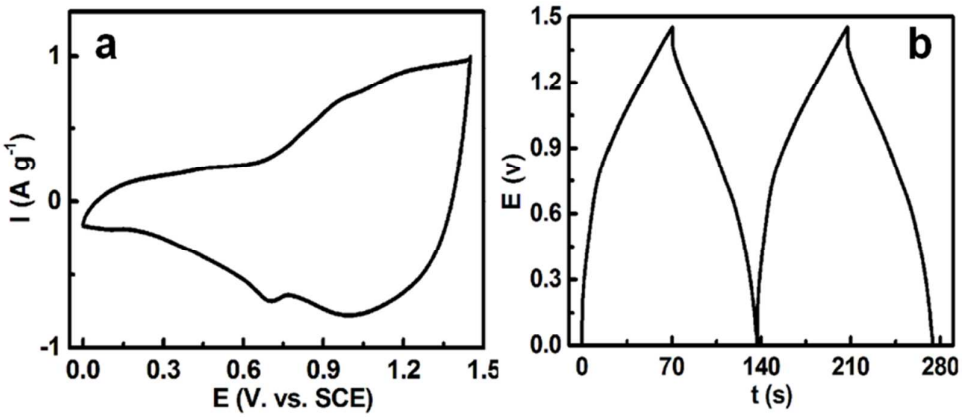

Figure 7 by Changzhou Yuan, *et al*.

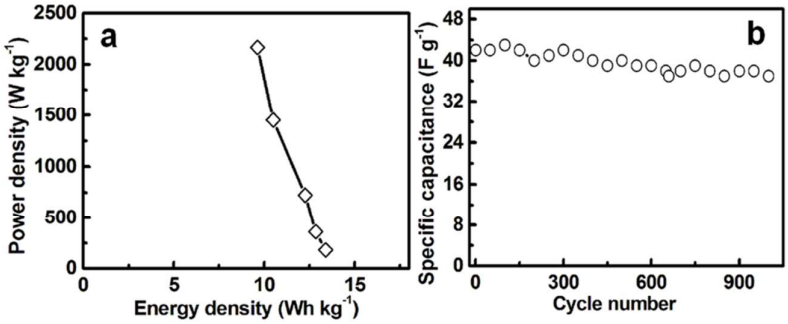

Figure 8 by Changzhou Yuan, *et al*.